Thermomodulation Spectra of Al, Au, and Cu†

R. Rosei* and D. W. Lynch
Institute for Atomic Research and Department of Physics, Iowa State University, Ames, Iowa 50010
(Received 10 January 1972)

Thermotransmission and thermoreflection measurements were made on semitransparent films of Al, Au, and Cu at about 370 and 120 K in the range 0.5–5 eV. The data yield the thermomodulation spectrum $\Delta\epsilon_2$ of the imaginary part of the dielectric constant directly, without Kramers-Kronig analysis. A comparison of the interband region of $\Delta\epsilon_2$ for Cu with the piezomodulation spectrum of a single crystal shows that broadening of the Fermi distribution and volume strain caused by thermal expansion are the principal causes of the $\Delta\epsilon_2$ spectrum. The $\Delta\epsilon_2$ spectrum for Al is particularly simple and can be discussed using closed-form expressions for the optical conductivity. It appears that the temperature dependence of the interband relaxation time for transitions across gaps produced by $|V_{111}|$ is smaller than that for transitions across gaps caused by $|V_{200}|$, which in turn is smaller than that for the infrared intraband transitions.

I. INTRODUCTION

Modulation spectroscopy, in which an oscillating perturbation is applied to a sample and the ac component of the reflected or transmitted light is measured, has proven to be a valuable way of precisely locating critical points in the interband absorption of solids.[1] In some cases,[2] the quantitative response of the solid to the perturbation has been measured. In this paper we describe thermomodulation measurements on several metals. The purpose of these measurements was to learn more about ways to make such measurements, to relate the results to other modulation measurements that are more straightforward to interpret, and to try to resolve some discrepancies in the interpretation of the optical properties of several metals.

In a thermomodulation measurement,[3–11] a small (perhaps 1–10 K) temperature wave is applied to the sample and the resultant ac component in the reflectivity R and/or transmission T is measured. These are called ΔR and ΔT, and they are directly proportional to the amplitude of the temperature wave as long as relative changes in temperature are small. It is difficult to interpret R and T spectra by themselves, because R and T are complicated functions of the real and imaginary parts of the dielectric constant, ϵ_1 and ϵ_2. This is equally true for the ΔR and ΔT spectra. The changes in ϵ_1 and ϵ_2, $\Delta\epsilon_1$ and $\Delta\epsilon_2$, are the proper spectra to interpret. Most previous thermomodulation measurements have been of $\Delta R/R$ for opaque samples. These have been Kramers-Kronig analyzed, after suitable extrapolations have been applied, to yield $\Delta\theta$, which is the change in the phase shift upon reflection due to the temperature change. $\Delta\epsilon_2$ can be found from $\Delta R/R$, $\Delta\theta$, ϵ_1, and ϵ_2. This method generally requires data over a wide frequency range. In the following we chose to work with films that were thin enough to be semitransparent. Both $\Delta R/R$ and $\Delta T/T$ were measured. If the thickness is also measured, $\Delta\epsilon_2$ can be obtained, again providing that ϵ_1 and ϵ_2 are known (see the Appendix). This has the advantages that data can be taken over a limited energy range, the resultant $\Delta\epsilon_1$ and $\Delta\epsilon_2$ can be checked independently by a Kramers-Kronig analysis (if suitable extrapolations can be made), and the film subsequently can be made thicker for measurements by the previously mentioned method. It has the disadvantages of introducing an additional measurement error (that of the thickness) and of requiring thinner films whose properties may not be as close to those of bulk samples.

Once a spectrum of $\Delta\epsilon_2$ is at hand, it should be interpreted. Unfortunately, thermomodulation is complicated. A small increase in temperature can alter the optical properties of a metal in a variety of ways.

(1) Volume thermal expansion decreases the plasma frequency and causes shifts and warping in the electron energy bands through changes in the one-electron potential. Changes in the bands cause the Fermi level to shift.

(2) If the sample is constrained by the substrate, thermal expansion also causes shear strains. These would not affect the free-electron gas, but they can split degenerate energy bands and cause shifting and warping as well. The latter could affect the Fermi level.

(3) The step in the Fermi distribution broadens. This affects all interband transitions that originate or terminate on states near the Fermi level.

(4) The phonon population increases. This decreases electron relaxation times and shifts and warps the energy bands through the electron-phonon interaction.

(5) The Fermi level increases even for a free-electron gas, but this is a small effect.

(6) If the temperature change is brought about by a current flow through the sample, the current flow

displaces the distribution function in k space.[12,13] Such an effect would be small, but it may be detectable in ideal cases.

All of these effects contribute to $\Delta\epsilon_2$ at a particular photon energy, if the band structure permits. The magnitude of the contribution depends on temperature as well as on the amplitude of the temperature wave. For example, effects (1) and (2) depend on the thermal expansion coefficient α, which is constant at high temperature and goes to zero as T^3 at low temperatures. Thus, independently of the detailed band structure of a given metal, changes are expected in the thermomodulation spectrum as the temperature is changed, changes that might be used to identify the microscopic origin of the spectrum. Effect (6) can be identified by a sensitivity to the direction of polarization of the measuring light with respect to the direction of current flow and by the fact that at high frequencies of modulation, all thermal effects should diminish (but not vanish), while the time constant for effect (6) should be of the order of 10^{-11} sec. It should also remain at low temperatures. Table I shows these contributions to the spectrum and how their amplitudes depend on temperature.

Given spectra of ϵ_2 and $\Delta\epsilon_2$ and a tentative band structure, one can identify features in the spectra and associate them with certain interband transitions. For shear strains, only those transitions that involve states well localized in k space, i.e., near certain critical points, give prominent features in the $\Delta\epsilon_2$ spectrum.[2] Volume strain causes these states and most states near any critical point to contribute to $\Delta\epsilon_2$, but it causes additional effects. Volume strain causes parallel bands to shift because of the volume dependence of a particular Fourier component of the pseudopotential. This will shift "parallel-band" (general-critical-point) absorption. Volume strain also causes a contribution to $\Delta\epsilon_2$ from those transitions between the Fermi level and a flat band. Thus the $\Delta\epsilon_2$ spectrum involves critical-point transitions as well as several other types of transitions. The shapes of the features in the $\Delta\epsilon_2$ spectrum help to identify the transitions. Cardona[14] has discussed the shapes of the $\Delta\epsilon_2$ spectra for critical-point transitions that are shifted or broadened by an increase in temperature. The analytical expressions for the shape of ϵ_2 arising from parallel-band absorption can be found in Refs. 15–19. They can be differentiated analytically or evaluated at two different temperatures to get $\Delta\epsilon_2$. The absorption between a flat band and the Fermi surface is discussed in Ref. 19.

II. EXPERIMENTAL

The samples were prepared by vacuum evaporation on flat, smooth, fused-quartz substrates, $1 \times 1 \times \frac{1}{16}$ in. The large substrates were chosen to avoid spurious signals due to sample motion or vibration. No such signals were ever found, so smaller substrates probably would have been successful. The samples were 2.5×10 mm and were several hundred Å thick. The thickness was measured with multiple-beam interference fringes and by optical-density measurements that were calibrated with the fringe measurements. The films were evaporated with an electron gun or a hot filament in a vacuum of better than 10^{-7} Torr. Several films were evaporated on single-crystal sapphire substrates.

The substrates were tightly clamped to the cold finger of a cryostat. Thermal contact was improved by a thin layer of vacuum grease. Leads were indium soldered to the ends of the film and a thermocouple was indium soldered to the substrate as close as possible to the film. The films were usually in a vacuum of 10^{-6} Torr within $\frac{1}{2}$ h of their removal from the evaporator.

The measuring system was rather conventional. Light sources were a tungsten-iodine lamp from 0.5 to 3.0 eV and a 150-W Xe arc above 3 eV. The light was sent through a Perkin-Elmer 99 prism double-pass monochromator and was focused on the sample. The chopper in the monochromator

TABLE I. Contributions to thermomodulation spectra and their temperature dependences. Θ is the "Debye" temperature, α is the thermal expansion coefficient, and f is the Fermi distribution function.

Effect	Temperature dependence of contribution to $\Delta\epsilon_2$		
	General	$T \gg \Theta$	$T \ll \Theta$
1. Isotropic thermal expansion	$\alpha(T)$	Constant	T^3
2. Shear strain from thermal expansion against substrate	$\alpha(T)$	Constant	T^3
3. Broadening of Fermi level	$\partial f/\partial T$		
4. Electron-phonon interaction	$(e^{\Theta/T}-1)^{-1}$	Constant	$e^{-\Theta/T}$
5. Shift of Fermi level	T	T	T
6. Current modulation	$\partial f/\partial T$		

was not used, but the slits were masked to obtain primarily double-passed light. Either reflected or transmitted light was then focused on the entrance slit of a Bausch and Lomb 250-mm grating monochromator used to filter out single-pass light. The detectors were a PbS cell for 0.5–2 eV, an RCA 7102 photomultiplier from 1 to 3 eV and an EMI 6256B photomultiplier from 2 to 5 eV.

Many different modulating-current wave forms and frequencies were used in an attempt to detect the current-modulation effect. The thermomodulation spectra reported below were all taken at 50 Hz by using square-wave modulation. A dc bias current was applied to keep the current unidirectional, which enabled 50-Hz detection. A Hewlett-Packard 202A was used as a signal generator, and a HP 467A as a power preamplifier. The 2–10-Ω sample was the load of a 2N3055 power transistor connected as an emitter follower. An Ithaco Model 353 lock-in amplifier was used. For small signals, a short-time constant was used and the output of the lock-in was fed to a voltage-to-frequency converter and a reversible counter for integration for times up to 10^3 sec. The dc signal from the detector was monitored and the detector supply voltage adjusted to keep this signal constant, which made the ac signal $\Delta T/T$ or $\Delta R/R$ directly.

Current-Modulation Effect

Although much effort was devoted to attempts to separate this effect from the purely thermal effects, no evidence for its existence was found. This effect can be identified by its frequency, polarization, and temperature dependence. Being an electronic effect, it should be frequency independent up to frequencies of the order of the inverse electron-relaxation time. Thermal effects display the well-known $1/\omega$ frequency dependence in the frequency range of interest. To push the modulation and detection to relatively high frequencies (120 kHz), a tuned-load photomultiplier was devised. The resonant frequency Ω of this device was accurately measured using a tiny fraction of the output of an amplitude-modulated laser. An unbiased sinusoidal signal of frequency $\frac{1}{2}\Omega$ was then used to modulate the sample. The lock-in amplifier detected the second harmonic. This configuration was used to minimize pickup, which is appreciable at high frequencies. No modulation signal above the noise level was detected at 120 kHz.

For a polycrystalline film with randomly oriented grains, or with crystallites having (100) or (111) axes normal to the plane of the film, the temperature-induced modulation of the transmission or the reflection should be independent of the state of polarization of normally incident measuring light, even when shear strains are produced.[20] The current flow through the sample lowers the symmetry and should give rise to a polarization dependence of the signal. No such dependence was found for films of Cu on fused-quartz substrates at 120 K, where light linearly polarized parallel and perpendicular to the current flow was used. A small difference was found for films on single-crystal sapphire substrates. This signal was reproducible, but extended to energies considerably below that of the signal due to the lowest-energy interband transition in Cu. This signal was an artifact of the sapphire substrates and may be the result of strain birefringence in the sapphire. These measurements were repeated at lower temperature to reduce all true thermoreflectance signals. Liquid helium was used as the refrigerant, but because of the large power dissipated in the samples, the average temperature of the samples was about 50 K and helium loss was very rapid. No current-modulation signal was detected.

III. RESULTS AND DISCUSSION

Gold

Scouler[6] carried out thermoreflectance measurements on gold, which were subsequently Kramers-Kronig analyzed by Cardona,[1] who also assigned transitions to the structures in $\Delta\epsilon_2$. The values of $\Delta\epsilon_1$ and $\Delta\epsilon_2$ derived from our measurements of $\Delta T/T$ and $\Delta R/R$ were used to calculate the $\Delta R/R$ spectrum of an opaque film of gold. The calculated spectrum was in good agreement with Scouler's results, so no further discussion is necessary. A detailed interpretation of the thermoreflectance spectrum of gold has been given by Christiansen and Seraphin.[21]

Copper

Copper probably has been the most widely studied metal. While great advances have been made in the last few years in understanding its optical properties, some controversy still exists as to the identification of some structures in the optical spectra.

The experimental results for two samples at different temperatures are shown in Figs. 1 and 2. The most striking features are

(1) a flat signal region (which, as in aluminum, is *not* an error signal) below the onset of interband transitions,

(2) a sharp derivative peak at about 2.15 eV,

(3) a rather broad structure in the range 2.4–3.6 eV, with a shoulder at 3.2 eV,

(4) a small, but reproducible, structure at 4 eV, and

(5) a very strong signal with twin peaks at 4.3 and 4.8 eV.

Figure 3 shows the computed $\Delta\epsilon_2$ for the 455-Å film at about 350 K. The $\tilde{\epsilon}$ data were from Pells and Shiga.[22,23] The free-electron region has been

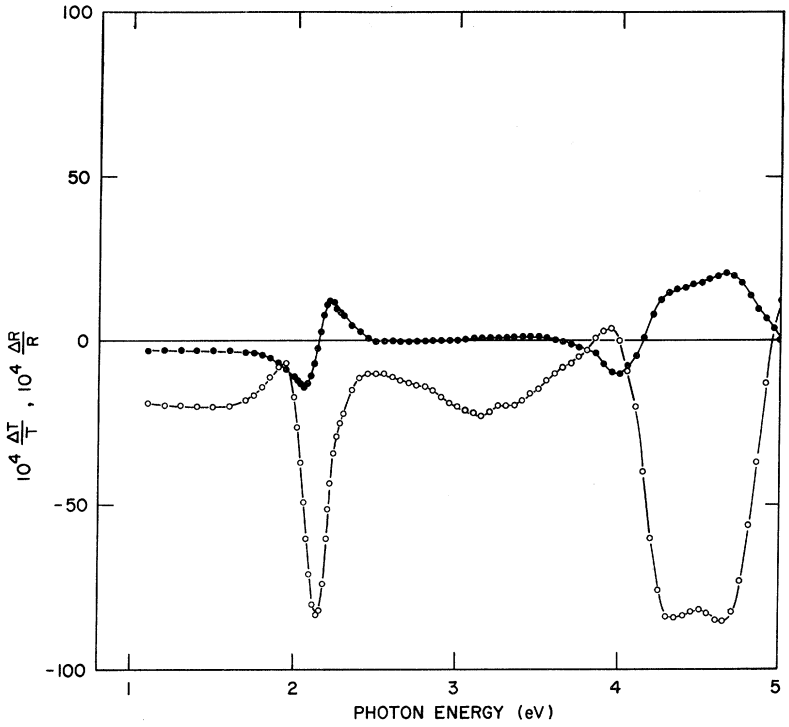

FIG. 1. Thermotransmission and thermoreflection spectra of a 455-Å-thick film of copper at about 350 K. Open circles represent $\Delta T/T$ and closed circles $\Delta R/R$. About 6 W of modulating power were dissipated in the sample.

fitted according to the free-electron model

$$\Delta\epsilon_2^{\text{free}} = A\,\Delta\omega_p + B\,\Delta\tau\ ,$$

where

$$A = \frac{2\omega_p\tau}{\omega(1+\omega^2\tau^2)}\ ,$$

$$B = \frac{\omega_p^2}{\omega(1+\omega^2\tau^2)}\ \frac{(1-\omega^2\tau^2)}{(1+\omega^2\tau^2)}\ .$$

The contribution of the plasma-frequency modulation is very small and has been neglected. Nevertheless, the fit is very good since in the region of interest ($\omega\tau \gg 1$) the coefficients A and B have substantially the same frequency dependence. The parameters used for the fit are

$$\hbar\omega_p = 9.3\ \text{eV}\ ,\quad \tau/\hbar = 30\ \text{eV}^{-1}\ ,\quad \Delta\tau/\hbar = 0.56\ \text{eV}^{-1}\ .$$

The error in $\Delta\tau$ caused by setting $\Delta\omega_p = 0$ has been estimated to be approximately 3%. With this value of $\Delta\tau$ and the data from Roberts,[24] it is possible to estimate the amplitude of the temperature modulation as ~12 K.

The onset of the first interband transition ($L_3 \rightarrow E_f$) at 2.15 eV is known to be almost temperature independent.[22,24,25] No shift is indeed detectable in the position of the experimental peaks at 120 and 350 K. A large part of this structure is due to the broadening of the Fermi distribution, as Cardona already has pointed out[1] for gold. The deformation potential for the $L_3 \rightarrow E_F$ transition is small.[2] Nevertheless the contribution of the modulation of the volume is important because of the very large value of $d\epsilon_2/dE$ in this region. This contribution

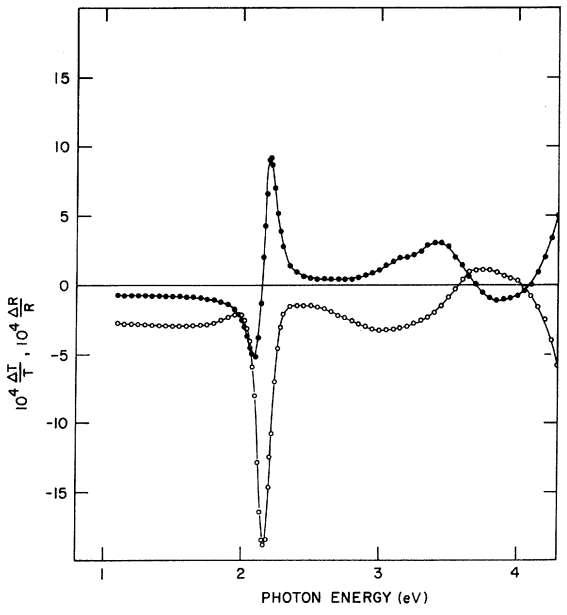

FIG. 2. Thermotransmission and thermoreflection spectra of a 310-Å-thick film of copper at about 120 K. Open circles represent $\Delta T/T$, and closed circles $\Delta R/R$. About 1.5 W of modulating power were dissipated in the sample.

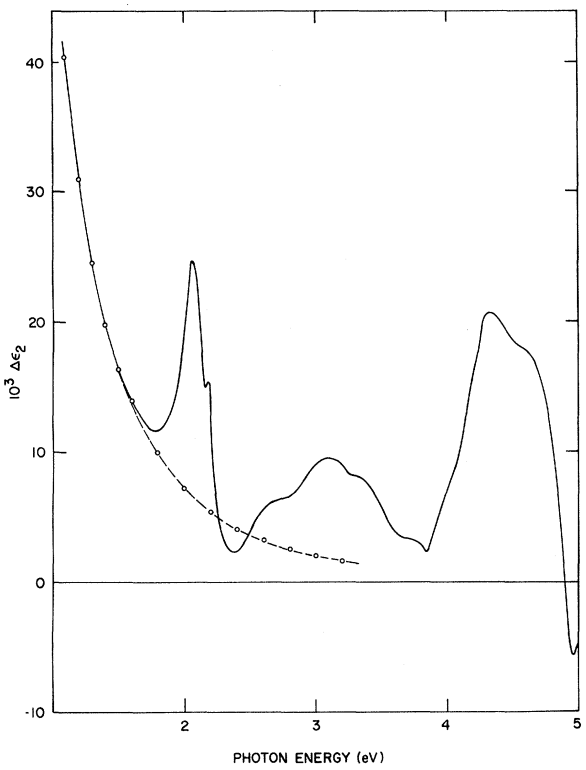

FIG. 3. $\Delta\epsilon_2$ spectrum resulting from the spectra in Fig. 1 (copper, ~350 K). The dashed line is a calculated spectrum for a free-electron gas as discussed in the text.

gives rise to the asymmetry on the derivative structure in Fig. 3. Figure 4 shows the results of a synthesis of this structure using a rough model based on the assumption of transitions from a flat d band to a parabolic conduction band.[19] In such a case,

$$\epsilon_2 \sim \frac{(E-E_0)^{1/2}}{E^2} \frac{1}{1+e^{(E-E_1)/k_BT}} \quad \text{for } E \geq E_0 ,$$

where E_0 is the difference in energy between the top of the flat d band and the bottom of the partly filled parabolic conduction band, and E_1 is the Fermi energy with respect to the top of the d band (Fig. 4). Straightforward differentation gives

$$\Delta\epsilon_2 = \left(\frac{\partial\epsilon_2}{\partial E_1}\right) \Delta E_1 + \left(\frac{\partial\epsilon_2}{\partial T}\right) \Delta T$$

$$\sim C(E, T)[\Delta E_1 + (E-E_1)\,\Delta T/T] ,$$

where ΔT is the amplitude of the temperature modulation, ΔE_1 is the change in E_1, and

$$C(E, T) = \frac{-1}{k_BT} \frac{\exp[(E-E_1)/k_BT]}{\{1+\exp[(E-E_1)/k_BT]\}^2} \frac{(E-E_0)^{1/2}}{E^2} .$$

The agreement with the experimental structure is only qualitative. This is not surprising since the model is oversimplified and does not take into account the contribution of higher-energy transitions. The data taken at low temperature support this interpretation. The shoulder at 2.15 eV (presumably

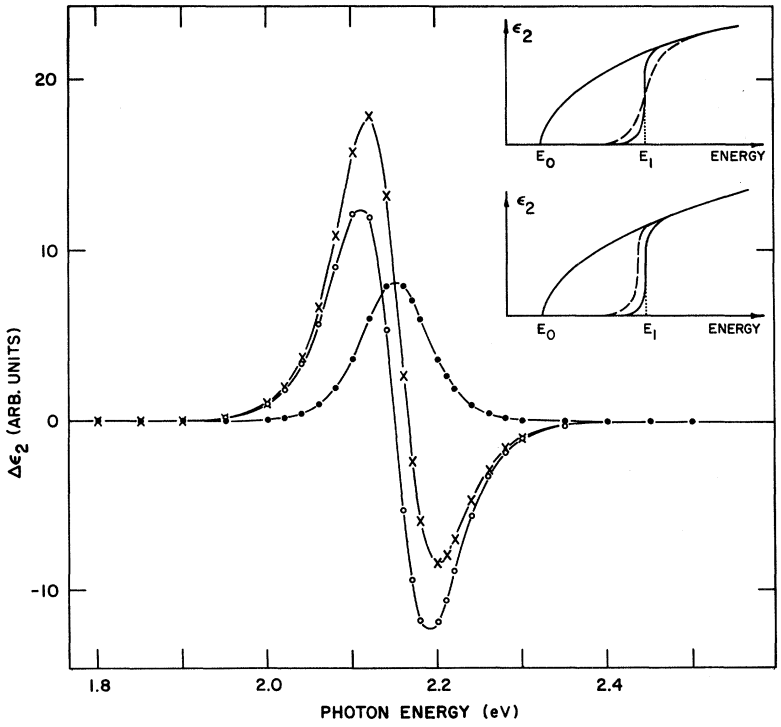

FIG. 4. Synthesis of the structure near 2.1 eV in Fig. 3 arising from 3d-band-edge-to-Fermi-level transitions. Open circles represent the contribution from the thermal broadening of the Fermi level. This is shown schematically in the upper right-hand inset, where the parabola represents the joint density of states. ϵ_2 begins near E_1 when Fermi statistics allow the transitions to occur. The onset of ϵ_2 is shown at two temperatures by the lines near E_1. Closed circles represent the contribution from the temperature shift of the 3d-band edge with respect to the Fermi level. The lower inset shows this process schematically. Crosses represent the total $\Delta\epsilon_2$, except for a free-electron term.

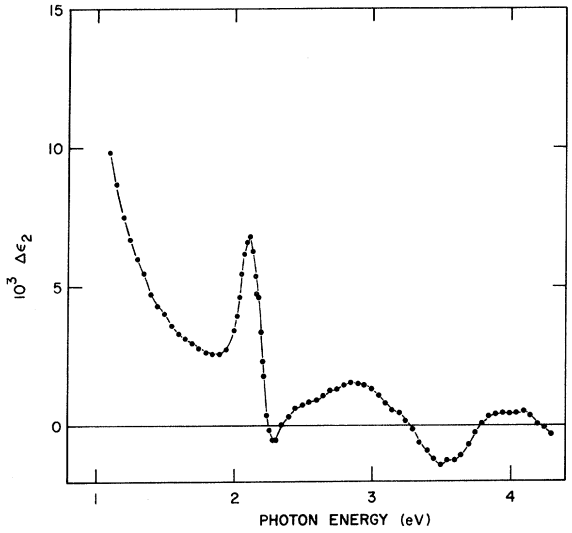

FIG. 5. $\Delta\epsilon_2$ spectrum resulting from the spectra in Fig. 2 (copper, ~120 K).

due to the peak of the volume contribution) has almost disappeared and the over-all structure is more symmetric (Fig. 5). At low temperature the volume modulation is, in fact, less important (see Table I). Fong *et al.*[26] have recently reported the wavelength-modulation spectrum of Cu single crystals at 7 K. Their spectrum shows more structural details than any previous derivative experiment. In particular, they see structure at 3.2 and 3.7 eV, which they attribute, respectively, to a volume effect and to an osculating point $(\Sigma_1 \rightarrow \Sigma_1)$ $(3 \rightarrow 6)$. Our thermoderivative spectrum also shows very similar structure at the same energies. One might expect a stronger thermoderivative signal for the osculating point at 3.7 eV. The lack of a marked response might be attributed to the nonflatness of the *d* band involved and does not necessarily mean that the assignment is incorrect.

Figure 6 compares (in arbitrary units) the high-energy results of the thermoderivative experiment with Gerhardt's data[2] for *isotropic* piezomodulation. As expected, the results are very similar. The shoulder at 4 eV in the thermoderivative data (not present in the isotropic modulation) is probably due to the shear stress modulation of the $X_5 \rightarrow X_4'$ transition. The shoulder at 4.7 eV is more pronounced in the thermoderivative experiment and then drops much faster. This strongly supports the interpretation of transitions from lower-lying *d* bands to the Fermi surface.

From the value of the peak in $\Delta\epsilon_2$ at 4.3 eV, it is possible to have an independent estimate for the amplitude of temperature modulation ΔT. Gerhardt[2] gives a value of 2.8 eV^{-1} for the derivative of the contribution of this transition to the total ϵ_2. From the value of 6.8×10^{-4} eV/K measured by Pells and Shiga[22] for the temperature dependence of the gap, we obtain $\Delta T = 10$ K, which is in very good agreement with the value obtained by fitting in the free-electron region.

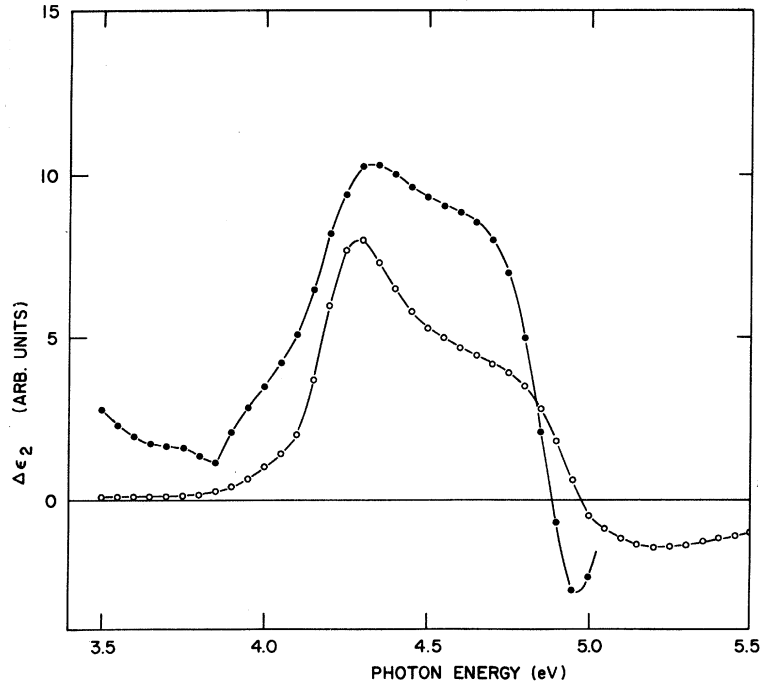

FIG. 6. Comparison of thermomodulation and volume modulation spectra in Cu. Closed circles represent the thermomodulation spectrum from Fig. 3. Open circles represent the $\Delta\epsilon_2$ due to hydrostatic volume strain (from Ref. 2).

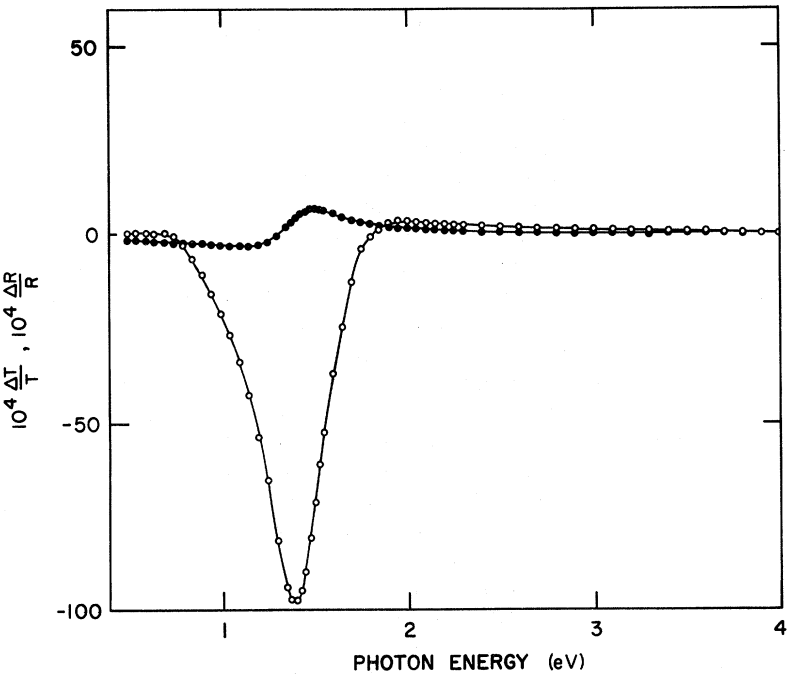

FIG. 7. Thermotransmission and thermoreflection spectra of a 310-Å-thick film of aluminum at about 370 K. Open circles represent $\Delta T/T$ and closed circles $\Delta R/R$. About 5 W of modulating power were dissipated in the sample.

Aluminum

The thermoderivative spectrum of aluminum is much simpler than that of Cu. As is shown in Figs. 7 and 8, it consists of (1) a flat signal region, as in copper, due to the intraband contribution and (2) a very-strong-signal region due to the well-known

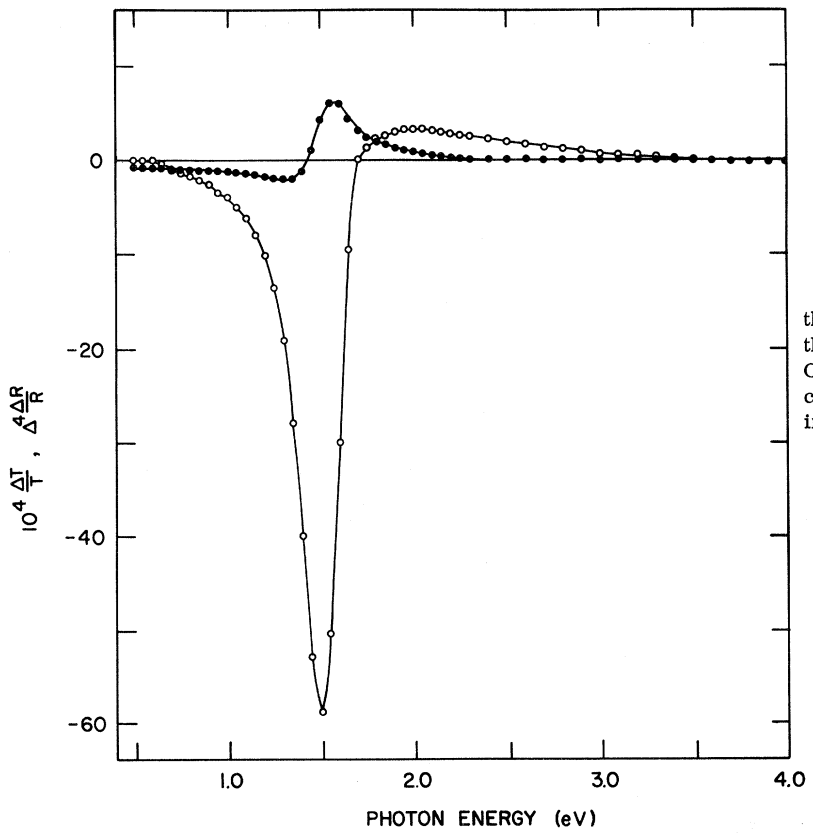

FIG. 8. Thermotransmission and thermoreflection spectra of a 290-Å-thick film of aluminum at about 120 K. Open circles represent $\Delta T/T$ and closed circles $\Delta R/R$. About 1.5 W of modulating power were dissipated in the sample.

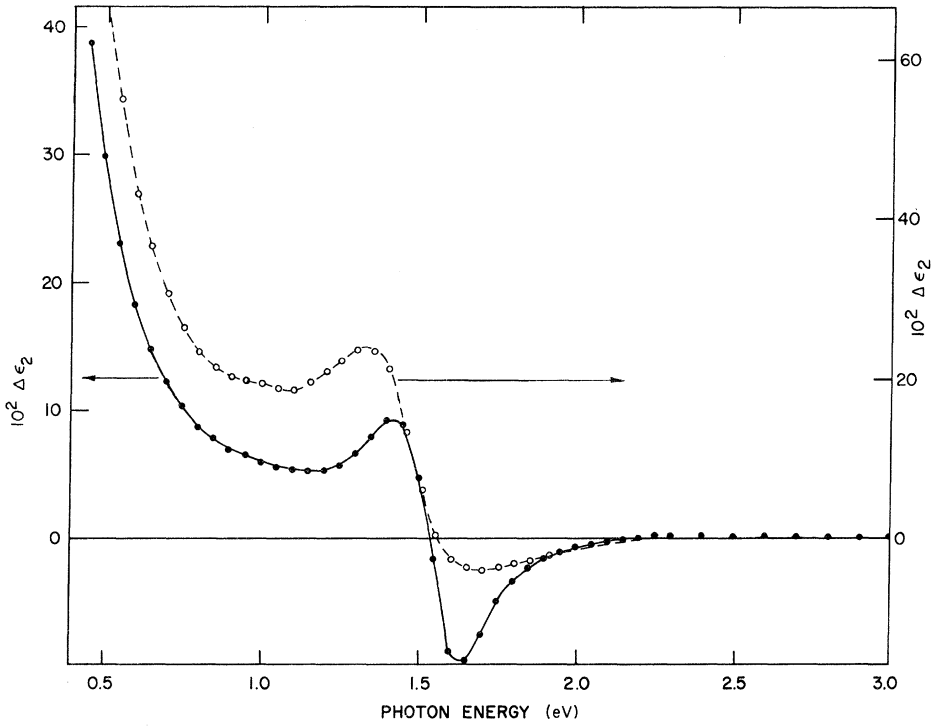

FIG. 9. $\Delta\epsilon_2$ spectra resulting from the spectra in Figs. 7 and 8. Open circles represent the film of Fig. 7, 370 K. Use right-hand scale. Closed circles represent film of Fig. 8, 120 K. Use left-hand scale.

interband absorption at 1.55 eV. The signal goes to zero above approximately 3 eV for both the modulated reflectivity and transmission, which shows that no error signal is present.

The modulated transmission signal is roughly an order of magnitude larger than the modulated reflectivity. This feature, in addition to the well-known sensitivity of modulation-spectroscopy techniques, makes our method particularly suitable for the detection of small structure. Nonetheless, it has not been possible to resolve the absorptivity peak at 0.52 eV theoretically predicted[18,27,28] and previously seen with a calorimetric technique.[29] The lack of structure in $\Delta T/T$ near 0.5 eV may be due to the reduced signal-to-noise ratio resulting from the very low transmission of the films at long wavelengths, or to the nonsensitivity of the 0.52-eV absorption peak to temperature (see below).

Figure 9 shows the $\Delta\epsilon_2$ spectra computed from our data for two samples at two temperatures. The necessary values of ϵ_2 were obtained from the work of Liljenvall, Mathewson and Myers[30,31] by using interpolation and extrapolation to obtain spectra at the temperatures we used. At low energy, a Drude term was used, even though this is expected to be of limited accuracy.[29] For ϵ_1 we were forced to use the room-temperature values of Ehrenreich *et al.*[32] The errors due to use of an improper ϵ_1 spectrum are difficult to estimate (see Appendix).

As can be seen in Fig. 9 the only structure near 1.5 eV is an asymmetric structure like the derivative of a single peak, which can be explained as arising from a single peak that shifts and broadens

TABLE II. Parameters used to fit $\Delta\epsilon_2$ at 120 K (Fig. 10).

Fixed	
$\lvert V_{111}\rvert$	0.216 eV
$\lvert V_{200}\rvert$	0.772 eV
$\tau_1/\hbar$	9.0 eV^{-1}
$\tau_2/\hbar$	9.0 eV^{-1}
$\tau_0/\hbar$	23.4 eV^{-1}
$\hbar\omega_p$	12.7 eV
$\Delta(\hbar\omega_p)$	0
Adjusted	
$\frac{-\Delta V_{111}}{\lvert V_{111}\rvert}$	$\lesssim 1.4\times10^{-4}$
$\frac{-\Delta V_{200}}{\lvert V_{200}\rvert}$	2.8×10^{-4}
$\frac{-\Delta\tau_{111}}{\tau_{111}}$	$\lesssim 0.5\times10^{-3}$
$\frac{-\Delta\tau_{200}}{\tau_{200}}$	2.0×10^{-3}
$\frac{-\Delta\tau_0}{\tau_0}$	5.5×10^{-3}

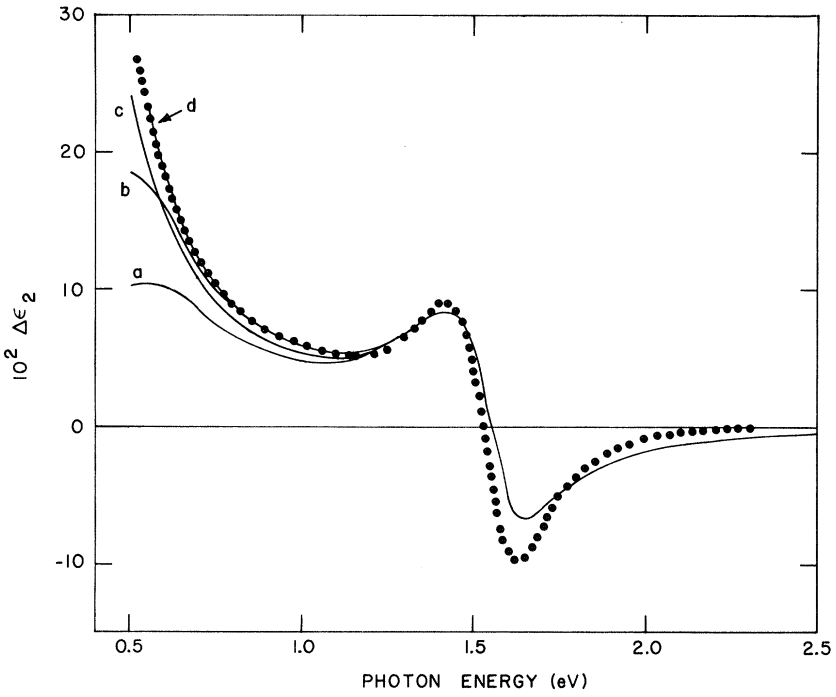

FIG. 10. Calculated $\Delta\epsilon_2$ spectrum (solid lines) and experimental $\Delta\epsilon_2$ spectrum (dotted line) for Al at 120 K. All computed curves have the parameters shown in Table II except for the values of $-\Delta V_{111}/|V_{111}|$ and $-\Delta\tau_{111}/\tau_{111}$, which are (a) 2.8×10^{-4} and 2.0×10^{-3}, (b) 0 and 2.0×10^{-3}, (c) 1.4×10^{-4} and 0.5×10^{-3}, and (d) 0 and 0. A computed curve with the parameters 2.8×10^{-4} and 0 lies almost on top of curve c.

with increasing temperature. There is no sign of any structure at 0.8, 1.2, and 1.45 eV as reported both in theoretical and experimental work.[33]

The interband absorption in Al is characterized by six parameters: the plasma frequency ω_p and relaxation time τ_0 of the free-electron gas, two Fourier coefficients $|V_{111}|$ and $|V_{200}|$ of the pseudopotential, and interband relaxation times τ_1 and τ_2 associated with each interband transition. Each of these parameters is temperature dependent, although ω_p can be viewed as constant in our spectral region, as it was for Cu. We have used the expression of Ashcroft and Sturm,[18] evaluated at two slightly different temperatures, to compute $\Delta\epsilon_2$ spectra for Al at 120 K. We fixed the values of $|V_{111}|$, $|V_{200}|$, τ_1, τ_2, and τ_0 by plotting $|V_j|$ and τ_j^{-1} vs temperature, using the values of Ref. 31. The curves were extrapolated roughly to 120 K (the lowest point in Ref. 31 was 198 K) and the resultant values, given in Table II, used as fixed constants. The values of $|V_{111}|$, τ_1, and τ_0 are less certain because of difficulties in fitting theoretical expressions over only a limited range of data.[31] The parameters ΔV_j and $\Delta\tau_j$ were first estimated from the slopes of the $|V_j|$ and $|\tau_j^{-1}|$ plots to correspond to a temperature change of 1 K. These were then adjusted to get a fit to the spectrum of Fig. 9 at 120 K. Several fits are shown in Fig. 10 and the final parameters are given in Table II. The ΔV_j and $\Delta\tau_j$ correspond to a decrease in both $|V_j|$ and τ_j with an increase in temperature. If we equate our value of $\Delta\tau_0/\tau_0$ to the dc value, we can estimate the amplitude of temperature modulation to be ~0.32 K from resistivity data[34] near 120 K. A similar argument leads to a modulation amplitude of ~3 K for the sample of Fig. 7 at 370 K.

It is clear that if $\Delta V_{111}/|V_{111}| = \Delta V_{200}/|V_{200}|$, observable structure due to the low-energy interband transition is predicted to persist to energies as high as 0.9 or 1.0 eV. Letting ΔV_{111} vanish does not remove structure calculated to be observable. Letting $\Delta\tau_1$ or both ΔV_{111} and $\Delta\tau_1$ vanish fits the data (Fig. 10), but because we cannot assign meaningful error estimates at low energy, we cannot say just how much smaller than our initial values ΔV_{111} and $\Delta\tau_1$ can be before they become consistent with the data.

It is difficult to improve the agreement near 1.5 eV beyond that achieved in Fig. 10. Increasing ΔV_{200} increases the positive peak at 1.4 eV much more than the negative peak at 1.6 eV. Increasing $\Delta\tau_2$ increases both peaks, but it significantly broadens the low-energy side of the 1.4-eV peak. Several combinations of ΔV_{200} and $\Delta\tau_2$ have been tried. In all cases the rapid return of the experimental $\Delta\epsilon_2$ spectrum to zero between 1.8 and 2.5 eV cannot be accounted for—all calculated spectra that give positive and negative peaks have too large a magnitude for $\Delta\epsilon_2$ above about 1.7 or 1.8 eV. To fit the $\Delta\epsilon_2$ spectrum above about 1.8 eV, $\Delta\tau_2$ may have to decrease with increasing energy. At 120 K, $\Delta\tau_1$ must be smaller than $\Delta\tau_2$ (and $\Delta\tau_1/\tau_1 < \Delta\tau_2/\tau_2$) and $\Delta\tau_2$ is less than $\Delta\tau_0$. $|V_{111}|$ must also be less temperature dependent than $|V_{200}|$.

IV. CONCLUSION

The method of making thermomodulation measurements described herein seems to be of general applicability if the films do not adhere well enough to their substrates to be given shear strain. Inaccuracies due to Kramers-Kronig analysis, especially important in modulation spectroscopy,[35] are avoided, but errors due to uncertainties in the absolute values of the dielectric constants are still present.

Thermomodulation spectra arising from transitions near symmetry critical points and general critical points (parallel bands) and from transitions from flat bands to the Fermi level have been seen. Their interpretation has been given qualitatively, but a detailed fitting of the shapes of the spectra is considerably complicated by the relatively large number of parameters used. The temperature coefficients of interband relaxation times are needed, as well as the coefficients of energy gaps.

ACKNOWLEDGMENTS

We wish to thank Professor H. P. Meyers for a report of Ref. 31 prior to publication, which facilitated the fitting of our aluminum spectra to theory, Dr. G. P. Pells for data on the optical constants of copper, and Dr. G. Dresselhaus for his computer program used to calculate ϵ_2 for Al in early stages of our data analysis.

APPENDIX

If a film of complex refractive index $\tilde{N} = n - ik$ and thickness d is on a transparent substrate of refractive index n_0, then at wavelength λ, the changes in n and k, Δn and Δk, can be calculated from the measured relative changes of transmission and reflection from the following expressions:

$$\tilde{\theta} = 2\pi i d/\lambda ,$$

$$\tilde{\rho} = \tilde{\theta}\,\tilde{N} ,$$

$$\tilde{X} = (n_0 + \tilde{N})(\tilde{N} + 1)\, e^{\tilde{\rho}} + (n_0 - \tilde{N})(\tilde{N} - 1)\, e^{-\tilde{\rho}} ,$$

$$\tilde{X}' = (n_0 - \tilde{N})(\tilde{N} + 1)\, e^{\tilde{\rho}} + (n_0 + \tilde{N})(\tilde{N} - 1)\, e^{-\tilde{\rho}} ,$$

$$\tilde{Y} = [(n_0 + 1 + 2\tilde{N}) + \tilde{\theta}(\tilde{N} + 1)(n_0 + \tilde{N})]\, e^{\tilde{\rho}} + [(n_0 + 1 - 2\tilde{N}) - \tilde{\theta}(\tilde{N} - 1)(n_0 - \tilde{N})]\, e^{-\tilde{\rho}} ,$$

$$\tilde{Y}' = [(n_0 - 1 - 2\tilde{N}) + \tilde{\theta}(\tilde{N} + 1)(n_0 - \tilde{N})]\, e^{\tilde{\rho}} + [(n_0 - 1 + 2\tilde{N}) - \tilde{\theta}(\tilde{N} - 1)(n_0 + \tilde{N})]\, e^{-\tilde{\rho}} ,$$

$$\tilde{Z} = \frac{1}{\tilde{N}} - \frac{\tilde{Y}}{\tilde{X}} ,$$

$$\tilde{Z}' = \frac{\tilde{Y}'}{\tilde{X}'} - \frac{\tilde{Y}}{\tilde{X}} ,$$

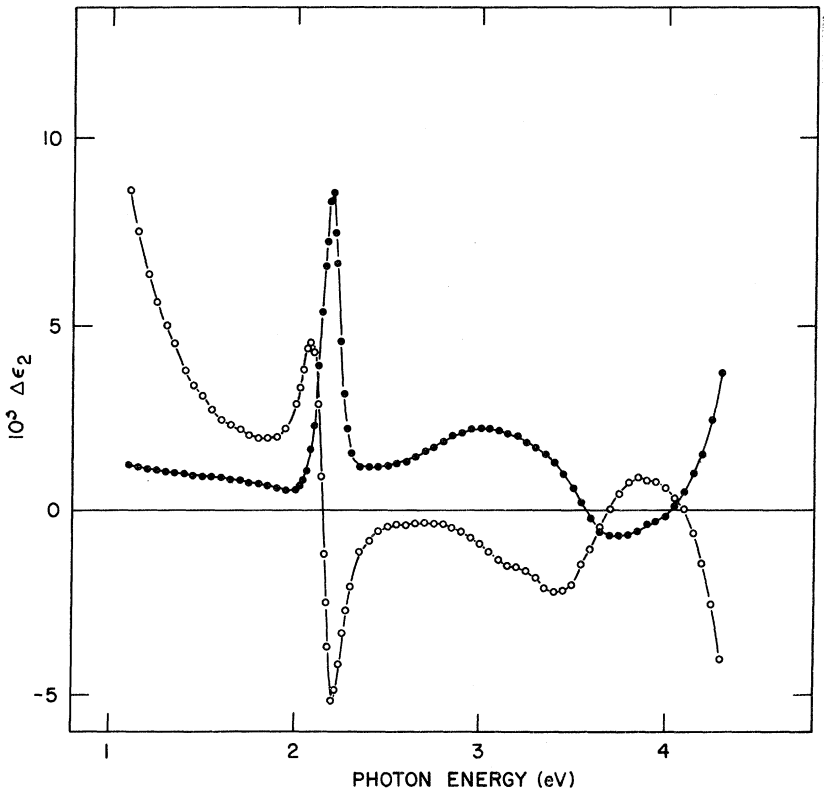

FIG. 11. $\Delta\epsilon_2$ spectrum of Fig. 5 resolved into two terms, one directly proportional to the measured $\Delta R/R$ (open circles) and the other directly proportional to $\Delta T/T$ (closed circles). Their sum is given in Fig. 5.

$$A=\mathrm{Re}\tilde{Z}\,,\quad B=\mathrm{Im}\tilde{Z}\,,\quad C=\mathrm{Re}\tilde{Z}'\,,\quad D=\mathrm{Im}\tilde{Z}'\,,$$

$$2\Delta n=\frac{B\,\Delta R/R-D\,\Delta T/T}{BC-AD}\,,$$

$$2\Delta k=\frac{A\Delta R/R-C\,\Delta T/T}{BC-AD}\,.$$

The changes in the real and imaginary parts of the dielectric constant are

$$\Delta\epsilon_1=2n\,\Delta n-2k\,\Delta k\,,\qquad \Delta\epsilon_2=2n\,\Delta n-2k\,\Delta k\,.$$

These expressions are valid for light that is normally incident from vacuum onto the film, not the substrate. It is also assumed that all relative changes are small enough that the quantities involving Δ's can be approximated by differentials. Reflection from the substrate-vacuum interface has been neglected, but a correction for this neglect would be to increase the measured $\Delta T/T$ by the factor $(n_0+1)^2/(n_0-1)^2$ before use in the equations. Multiple reflections in the film have been included, but with interference fringes averaged out.

Errors in $\Delta R/R$ and $\Delta T/T$ are only a few percent in the present work because of long integration times and repeated scans. The error in d may be as high as 10%. We have allowed the value of d to vary by 10% in analyzing the data of Fig. 7. The resulting $\Delta\epsilon_2$ spectrum did not differ qualitatively from that of Fig. 9. The height of the positive peak decreased 5% and that of the negative peak increased 3% when d was increased 10%. Changes outside the 1–2-eV range were less than 1%.

The largest single source of error is probably in the values of n and k. In comparing the data of several authors, one usually finds the same shapes for the spectra of n and k, but the magnitudes may vary by 50% or more. (This dependence on the accuracy of the values of n and k also occurs when Kramers-Kronig analysis of $\Delta R/R$ is performed.) Moreover, the two terms in the final expression for $\Delta\epsilon_2$ often have opposite signs, so that they tend to cancel. This makes the error in $\Delta\epsilon_2$ very difficult to estimate.

Figure 11 shows the $\Delta\epsilon_2$ spectrum of Fig. 5 broken into the two components

$$\frac{(nB-kA)}{(BC-AD)}\,\frac{\Delta R}{R}\quad\text{and}\quad\frac{-(nD-kC)}{(BC-AD)}\,\frac{\Delta T}{T}\,.$$

It is clear that errors in the magnitudes of n and k could cause distortions in the structure of the $\Delta\epsilon_2$ spectrum. Such errors are difficult to assess and no attempt was made to use different sets of optical data on copper to test for sensitivity. For other metals a variety of published spectra often does not exist.

---

†Work performed at the Ames Laboratory of the U. S. Atomic Energy Commission, Contribution No. 3178.

*Present address: Istituto di Fisica dell'Universitá, Roma, Italy.

[1]M. Cardona, *Solid State Physics*, edited by F. Seitz, D. Turnbull, and H. Ehrenreich (Academic, New York, 1969), Suppl. 11.

[2]U. Gerhardt, Phys. Rev. 172, 651 (1968).

[3]B. Batz, Solid State Commun. 4, 241 (1965).

[4]C. N. Berglund, J. Appl. Phys. 37, 3019 (1966).

[5]B. Batz, Solid State Commun. 5, 985 (1967).

[6]W. J. Scouler, Phys. Rev. Letters 18, 455 (1967).

[7]J. Hanus, J. Feinleib, and W. J. Scouler, Phys. Rev. Letters 19, 16 (1967).

[8]E. Matatagui and M. Cardona, Solid State Commun. 6, 313 (1968).

[9]A. Balzarotti and M. Grandolfo, Phys. Rev. Letters 20, 9 (1968).

[10]A. Balzarotti and M. Grandolfo, Solid State Commun. 6, 815 (1968).

[11]G. Baldini and M. Nobile, Solid State Commun. 8, 7 (1970).

[12]C. A. Baumgardner and T. O. Woodruff, Phys. Rev. 173, 746 (1968).

[13]C. V. Hodge and C. A. Baumgardner, Phys. Rev. B 1, 3347 (1970).

[14]Reference 1, Secs. 10 and 17.

[15]W. A. Harrison, Phys. Rev. 142, 467 (1966).

[16]R. N. Gurzhi and G. P. Motulevich, Zh. Eksperim. i Teor. Fiz. 51, 1220 (1966) [Sov. Phys. JETP 24, 818 (1967)].

[17]A. I. Golovashkin, A. I. Kopeliovich, and G. P. Motulevich, Zh. Eksperim. i Teor. Fiz. 53, 2053 (1967) [Sov. Phys. JETP 26, 1161 (1968)].

[18]N. W. Ashcroft and K. Sturm, Phys. Rev. B 3, 1898 (1971).

[19]B. R. Cooper, H. Ehrenreich, and H. R. Phillipp, Phys. Rev. 138, A494 (1965).

[20]M. Garfinkel, J. J. Tiemann, and W. E. Engeler, Phys. Rev. 148, 968 (1966).

[21]N. E. Christensen and B. O. Seraphin, Solid State Commun. 8, 1221 (1970); Phys. Rev. B 4, 3321 (1971).

[22]G. P. Pells and M. Shiga, J. Phys. C 2, 1835 (1969).

[23]G. P. Pells (private communication).

[24]S. Roberts, Phys. Rev. 118, 1509 (1960).

[25]R. Zallen, in *Optical Properties and Electronic Structure of Metals and Alloys*, edited by F. Abeles (North-Holland, Amsterdam, 1966), p. 164.

[26]C. Y. Fong, M. L. Cohen, R. R. L. Zucca, J. Stokes, and Y. R. Shen, Phys. Rev. Letters 25, 1486 (1970).

[27]D. Brust, Phys. Rev. B 2, 818 (1970).

[28]A. J. Hughes, D. Jones, and A. H. Lettington, J. Phys. C 2, 102 (1969).

[29]L. W. Bos and D. W. Lynch, Phys. Rev. Letters 25, 156 (1970).

[30]H. G. Liljenvall, A. G. Mathewson, and H. P. Myers,

Solid State Commun. 9, 169 (1971).
[31]A. G. Matheson and H. P. Myers (unpublished).
[32]H. Ehrenreich, H. R. Philipp, and B. Segall, Phys. Rev. 132, 1918 (1963).
[33]G. Dresselhaus, M. S. Dresselhaus, and D. Beaglehole, in *Proceedings of the Third Materials Research Symposium* (Natl. Bur. Std., Gaithersburg, Md., to be published).
[34]G. T. Meaden, *Electrical Resistance of Metals* (Plenum, New York, 1965).
[35]B. F. Schmidt and D. W. Lynch, Phys. Rev. B 3, 4015 (1971).

PHYSICAL REVIEW B VOLUME 5, NUMBER 10 15 MAY 1972

Inversion of Fermi-Surface Data Using Partial-Wave Phase Shifts and Their Derivatives: An Application to the Noble Metals*

Jerry C. Shaw, J. B. Ketterson, and L. R. Windmiller
Argonne National Laboratory, Argonne, Illinois 60439
(Received 15 October 1971)

Utilizing the Korringa-Kohn-Rostoker method, we present straightforward procedures for efficiently parametrizing experimental Fermi-surface data. Useful techniques, derived from standard least-squares methods, are generated for fitting areas, cyclotron effective masses, and pressure derivatives of areas, using as adjustable parameters, phase shifts, energy derivatives of phase shifts, and lattice-constant derivatives of phase shifts, respectively. We apply these techniques to recent noble-metal Fermi-surface data and demonstrate that the quality of fit for the above quantities is highly insensitive to the assumed value of the energy parameter used in the formalism.

I. INTRODUCTION

It has recently been suggested by Segal and Ham[1] and demonstrated by Lee[2–4] and Cooke, Davis, and Wood[5] and the present authors[6] that the anisotropy of de Haas–van Alphen (dHvA) data may be accurately parametrized utilizing as adjustable parameters energy-independent partial-wave-scattering phase shifts. The energy-dependent form of the phase shifts, $\eta_l(E)$, characterize the scattering of electrons due to the "muffin-tin" potential used in the augmented-plane-wave (APW)[7] and Korringa-Kohn-Rostoker (KKR)[8,9] methods of calculating electronic dispersion curves.

The advantages of this method are several-fold, but most important is the rapid convergence of the formalism to allow accurate characterization of the data in terms of a few parameters. For example, copper data may be quite accurately fitted using only three phase shifts corresponding to s, p, and d angular-momentum states. This compares with the seven nonphysical parameters used in the Fourier-series techniques[10–12] for the noble metals. For highly distorted surfaces, either Fourier-series techniques[12–14] or, if it is a closed centrosymmetric surface, a series of symmetrized spherical harmonics,[15] require many coefficients to describe the anisotropy of a single sheet. Conceivably, a multiple-sheet Fermi surface can be parametrized using a single set of three or four η_l's; we shall present in a later paper results for fits for such metals, including the effects of spin-orbit coupling.

The energy used to characterize the Fermi surface in this formalism is measured relative to the value of the constant potential in the interatomic region, i.e., $E = E_F - V_{MTZ}$, where E_F is the Fermi energy and V_{MTZ} is the constant potential. Workers have observed a nonunique relationship between the phase shifts and the value of E that give reasonable fits to dHvA data. Preliminary numerical studies[6] suggested that a family of phase shifts versus E could be generated which give accurate fits to dHvA data over a large range of E. Recent attempts to resolve this ambiguity have been made by Andersen[16] and by Heine and Lee.[17] In Sec. III, we give strong numerical evidence to support the contention that the quality of fit to dHvA data is intrinsically E independent and that any E dependence is due to the effects of truncating the order of the secular matrix, i.e., the lack convergence of the formalism resulting from the use of a finite number of phase shifts.

In Sec. II, we describe general techniques, using the KKR formalism, for rapidly determining parameters from a given set of experimental data. In Secs. III–V we describe specific procedures for calculating theoretical quantities, either using a first-principles potential or as functions of adjustable parameters. In each section we present the results of the application of the parametrization schemes to recent data for the noble metals. Finally, in Sec. VI, we present a summary and conclusions, while in the Appendix, we describe straightforward pro-